# Chapter 4
# Primary Creep


**Abstract** For many materials, primary creep can be described with the phi ($\phi$) model and tertiary creep with the Omega ($\Omega$) model (discussed in Chap. 12). According to the phi model, the creep rate is linear in strain and time in a double logarithmic diagram. When using empirical descriptions of the creep curves, these models are recommended. Several basic models for primary creep are derived. They are based on the creep rate in the secondary stage. This means that primary creep can be derived without any new data. The primary creep models are in agreement with the phi model and can describe experimental data. For the martensitic 9–12% Cr steels at least two dislocation densities are needed to represent primary creep because the initial dislocation density is high contrary to the situation for annealed fcc materials.

## 4.1 General

The classical form of a creep strain versus time curve ("creep curve") is that there is first a primary stage where the creep rate increases but with a continuously decreasing rate, a secondary stage where the creep rate is approximately constant and a tertiary stage with a continuously increasing strain rate. Surprisingly many materials show this behavior but there are many exceptions. In this chapter the primary stage will be analyzed.

The primary stage is technically very important. If there is a limit on the amount of strain that a product can accept, primary creep must be considered. Well-known examples are blades of gas and steam turbines. If the strain is too large the blades will get in contact with other parts of the structure resulting in disaster. Another case is where the strains can never become very large. One example is copper canisters for nuclear waste. Inside the copper tube there is a cast iron insert. Between the copper tube and the iron insert there is only a small gap. Due to the external pressure the copper tube creeps towards the insert and when it is reached, creep stops in this part of the structure. For some materials the total strain is larger in the primary stage than in the secondary stage. If only secondary creep is considered in design which is not uncommon, there is a risk that the creep deformation is significantly underestimated.



R. Sandström, *Basic Modeling and Theory of Creep of Metallic Materials*, Springer Series in Materials Science 339,
https://doi.org/10.1007/978-3-031-49507-6_4

Primary creep is also of importance during creep at very low stresses since stationary conditions are rarely reached. This is discussed in Chap. 5.

Secondary creep has been studied much more extensively than primary creep in the literature. The reason is that for a long time it was believed that the stress exponent in the secondary stage could be used to identify the controlling creep mechanisms. As was discussed in Chap. 2 and will be further discussed in Chap. 5, this connection is not always true and examples where people are likely to have drawn the wrong conclusions are easy to find.

Primary creep has almost exclusively been analyzed with empirical models. Only in recent years, basic models have been presented in the literature. Already in the 1930'ties, Bailey presented a model for the time dependence of the strain in primary creep. This model is still the first hand choice when describing the primary stage. The model has later been generalized [1]. We will refer to it as the phi or $\phi$ model. It gives an exponential decrease in creep rate with increasing time or strain. As will be illustrated in the next section several types of materials follow this behavior.

There are a large number of empirical models for representing creep curves. Only a few of them give a reasonable description of primary and tertiary creep separately and we will focus on them. For tertiary creep, the correspondence to the phi ($\phi$) model is the Omega ($\Omega$) model. These two models can accurately represent primary and tertiary creep for the well investigated 9CrMo steels.

Basic models for primary creep have been developed in recent years. Three of these models will be presented in Sects. 4.3–4.5. The first two models are applicable to fcc alloys whereas the third one is suitable for CrMo-steels. In some of the models it is necessary to distinguish between more than one type of dislocation density. In general these models give the same time dependence of the strain as the phi ($\phi$) model. Expressed in other words, the phi ($\phi$) model can be derived from basic physical principles, which has not been shown for any other of the empirical model for primary creep. So this is an additional reason why we concentrate on the phi ($\phi$) model, when discussing empirical models for primary creep.

## 4.2 Empirical Models for Creep Strain Curves

In this section models for both primary and tertiary creep will be considered. The reason is that many models are designed to handle the entire creep curve rather than primary and tertiary creep separately. A large number of empirical models have been proposed. Reviews can be found in [2, 3]. Some of the more frequently used methods are summarized in Table 4.1. The model that probably has got most attention in the literature was developed by the Wilshire group. They referred to it as $\theta$ projection. In Table 4.1 it is called the $\theta$ model. The assumptions in the model are that both the primary and the tertiary creep rates are linear in the creep strain. This gives a creep rate that decreases exponentially with time in the primary stage and increases exponentially in the tertiary stage. To describe the whole creep curve the primary and tertiary parts are simply added. Thus, it is not necessary to have a separate contribution

from secondary creep. However, if primary and tertiary data are analyzed separately, the θ model does typically not give a good representation of data.

Instead the ϕ model should be used for primary creep data and the Omega (Ω) model for tertiary data. This will be illustrated below. The phi (ϕ) model for primary creep gives the following strain rate dependence as a function of strain

$$\dot{\varepsilon}_{\text{prim}} = \phi_1 \varepsilon^{-\phi_2} \qquad \text{phi model} \tag{4.1}$$

The creep rate decreases exponentially with increasing strain. Its time dependence has the same mathematical form. The Ω model for tertiary creep takes the form

$$\dot{\varepsilon}_{\text{tert}} = \Omega_3 e^{\Omega_4 \varepsilon} \qquad \text{Omega model} \tag{4.2}$$

In Eq. (4.2) the creep rate increases exponentially with strain. This gives a time dependence with a singularity, see Table 4.1. The time at this singularity is close to the rupture time.

The three models in Table 4.1 have one term for primary creep and one for tertiary creep. In each term there are two adjustable parameters. So for describing a creep curve four adjustable parameters are needed.

Equations (4.1) and (4.2) are illustrated for the 9Cr1Mo steel P91 in Figs. 4.1, 4.2, 4.3 and 4.4. The steel P91 is common in modern fossil fired power plants.

**Table 4.1** Empirical models for describing single creep curves (reproduced from [4] with permission of Elsevier)

| Model | Parameters | Strain rate versus strain | Strain rate versus time | Strain versus time | Refs. |
|---|---|---|---|---|---|
| θ model, primary | $\theta_1, \theta_2$ | $\dot{\varepsilon}_{\text{prim}} = \theta_2(\theta_1 - \varepsilon)$ | $\dot{\varepsilon}_{\text{prim}} = \theta_1\theta_2 e^{-\theta_2 t}$ | $\theta_1(1 - e^{-\theta_2 t})$ | [5, 6] |
| θ model, tertiary | $\theta_3, \theta_4$ | $\dot{\varepsilon}_{\text{tert}} = \theta_4(\varepsilon + \theta_3)$ | $\dot{\varepsilon}_{\text{tert}} = \theta_3\theta_4 e^{\theta_4 t}$ | $\theta_3(e^{\theta_4 t} - 1)$ | [5, 7] |
| ϕ model, primary | $\phi_1, \phi_2$ | $\dot{\varepsilon}_{\text{prim}} = \phi_1 \varepsilon^{-\phi_2}$ | $\dot{\varepsilon}_{\text{prim}} = \phi_1(\phi_1(1+\phi_2)t)^{-\phi_2/(1+\phi_2)}$ | $(\phi_1(1+\phi_2)t)^{1/(1+\phi_2)}$ | [1, 8] |
| ϕ model, tertiary | $\phi_3, \phi_4$ | $\dot{\varepsilon}_{\text{tert}} = \phi_3 \varepsilon^{\phi_4}$ | $\dot{\varepsilon}_{\text{tert}} = \phi_3(\phi_3(1-\phi_4)t)^{\phi_4/(1-\phi_4)}$ | $(\phi_3(1-\phi_4)t)^{1/(1-\phi_4)}$ | [8] |
| Ω model, primary | $\Omega_1, \Omega_2$ | $\dot{\varepsilon}_{\text{prim}} = \Omega_1 e^{-\Omega_2 \varepsilon}$ | $\dot{\varepsilon}_{\text{prim}} = \frac{\Omega_1}{\Omega_1\Omega_2 t+1}$ | $\frac{\ln(\Omega_1\Omega_2 t+1)}{\Omega_2}$ | [9] |
| Ω model, tertiary | $\Omega_3, \Omega_4$ | $\dot{\varepsilon}_{\text{tert}} = \Omega_3 e^{\Omega_4 \varepsilon}$ | $\dot{\varepsilon}_{\text{tert}} = \frac{\Omega_3}{1-\Omega_3\Omega_4 t}$ | $-\frac{\ln(1-\Omega_3\Omega_4 t)}{\Omega_4}$ | [10–12] |

ε is the creep strain, $\dot{\varepsilon}$ the strain rate, $t$ the time

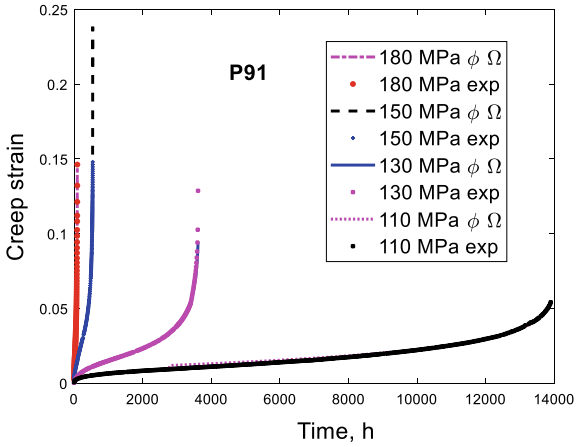


**Fig. 4.1** Creep strain versus time curves for the 9Cr1Mo steel P91 at 600 °C at the four stresses 110, 130, 150 and 180 MPa fitted with the ϕ and Ω models, Eqs. (4.1) and (4.2). Data from [1]. Reprinted from [13] with permission of MDPI

By using double logarithmic scale for a creep rate versus strain curve, a straight line should result in the primary stage if Eq. (4.1) is valid. That this is the case is shown in Fig. 4.2.

The same behavior can be illustrated if the creep rate is plotted versus time. From Table 4.1 it can be seen that also the time dependence of the creep rate in the primary stage is exponential. It should give a straight line in Fig. 4.3. This is approximately the case. However, this way of presenting the data is more sensitive to the scatter in the data.

In the tertiary stage a semi logarithmic scale with the creep rate versus strain diagram is appropriate to make a comparison to the Omega (Ω) model in Eq. (4.2).

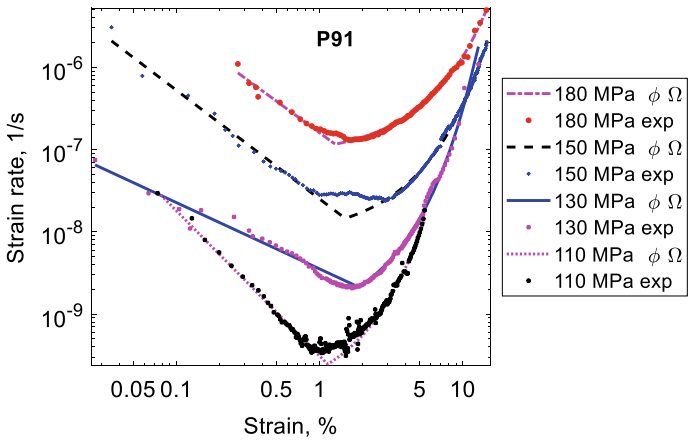


**Fig. 4.2** Creep rate versus strain curves for the 9Cr1Mo steel P91 at 600 °C for the same tests as in Fig. 4.1. Double logarithmic scale. Reprinted from [13] with permission of MDPI

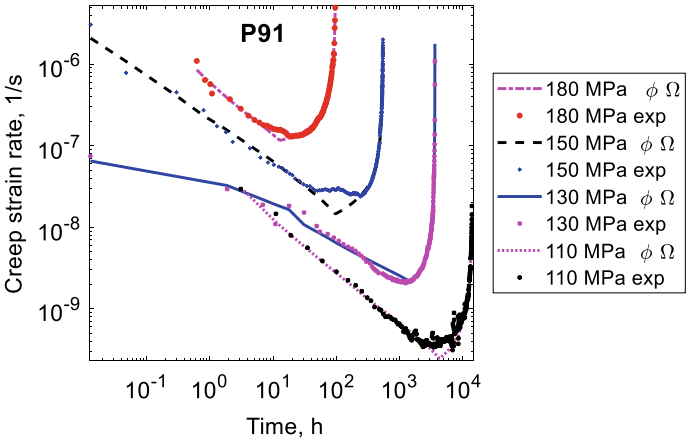


**Fig. 4.3** Creep rate versus time curves for the 9Cr1Mo steel P91 at 600 °C for the same tests as in Fig. 4.1. Double logarithmic scale

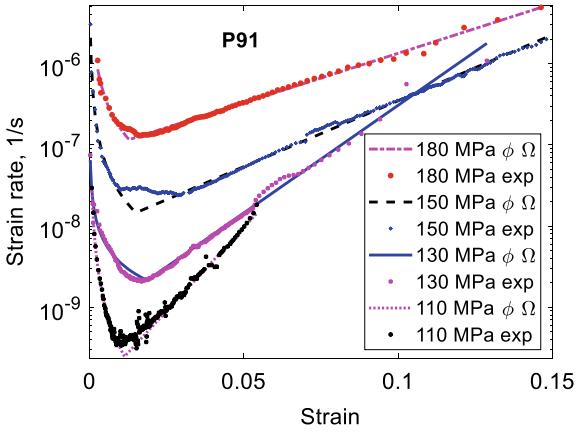


**Fig. 4.4** Creep rate versus strain curves for the 9Cr1Mo steel P91 at 600 °C for the same tests as in Fig. 4.1. Semi logarithmic scale. Data from [14]. Reprinted from [13] with permission of MDPI

This is illustrated in Fig. 4.4. Indeed, straight lines give a good representation of the data. Some deviations around the minimum creep rate can be observed.

In Figs. 4.2, 4.3 and 4.4 the contributions from both Eqs. (4.1) and (4.2) are included. The maximum value of them is shown. It can be seen that the whole curves are quite well represented in this way.

Also the strain versus time curve in Fig. 4.1 can be handled in this way. For the primary stage Eq. (4.1) is used and for the tertiary stage Eq. (4.2). If an even better fit is required for the strain versus time curve all the parameters $\phi_1$, $\phi_2$, $\Omega_3$ and $\Omega_4$ can be fitted simultaneously to the data. In fact, if four parameters are fitted many combinations of models for primary and tertiary can be used, for example different combinations in Table 4.1 such as the $\theta$ model or the $\Omega$ model for both primary and tertiary creep. However, such an approach is not recommended because

the expressions for the primary and tertiary stages will not be able to describe the primary and the tertiary stages separately.

It is well established that high chromium steels like P91 follows the ϕ model in the primary stage and the Ω model in the tertiary stage at least approximately. This is well documented in the literature. For example, Abe has written several papers about it [15–18]. The phi (ϕ) and Omega (Ω) models are also applicable to other types of materials. This will be illustrated in Figs. 4.5, 4.6, 4.7 and 4.8 for the high alloyed creep resistant austenitic stainless steel Sanicro 25 (22Cr25Ni4W1.5Co3CuNbN) developed by Sandvik.

Creep strain versus time curves are shown in Fig. 4.5. It can be noticed that the appearance of the creep curves is quite different from those of P91. The amount of primary creep is quite small and tertiary creep starts early on and dominates the creep curve.

In Fig. 4.6, strain rate versus time curves with a double logarithmic scale are given. The presence of the straight lines in the primary stage illustrates that the phi (ϕ) model is satisfied for three of the stresses.

Also in creep rate versus time curves the validity of the ϕ model can be demonstrated, see Fig. 4.7. Due to scatter in the experimental data the agreement is not complete.

For the primary stage only a limited number of data points on the creep curves are available in [19]. For the tertiary stage the data situation is much better. It is evident in Fig. 4.8 that the tertiary is well represented by the Omega (Ω) model.

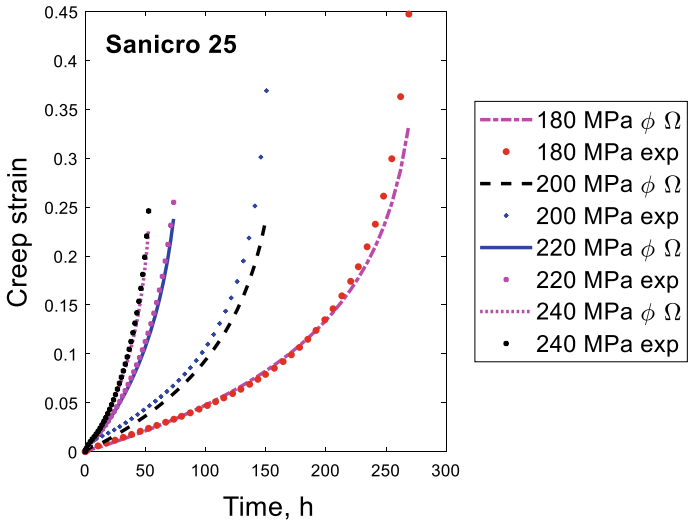


**Fig. 4.5** Creep strain versus time curves for the 22Cr25Ni4W1.5Co3CuNbN austenitic stainless steel Sanicro 25 at 750 °C at the four stresses 180, 200, 220 and 240 MPa fitted with the ϕ and Ω models, Eqs. (4.1) and (4.2). Data from [19]. Reprinted from [13] with permission of MDPI

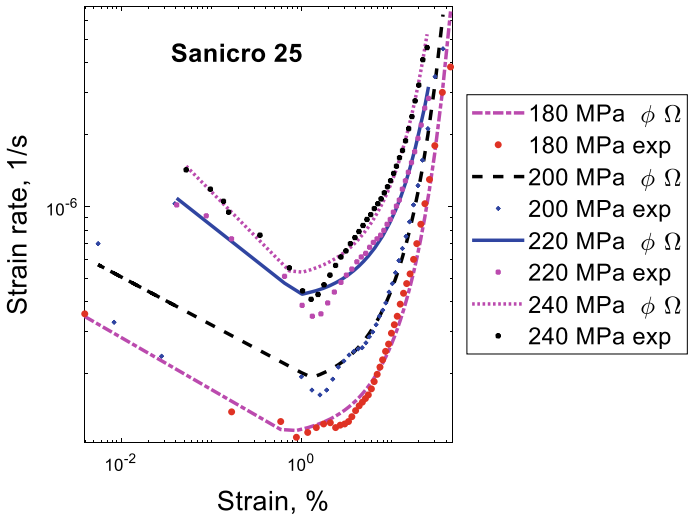


**Fig. 4.6** Creep rate versus strain curves for the 22Cr25Ni4W1.5Co3CuNbN austenitic stainless steel Sanicro 25 at 750 °C for the same tests as in Fig. 4.5. Double logarithmic scale

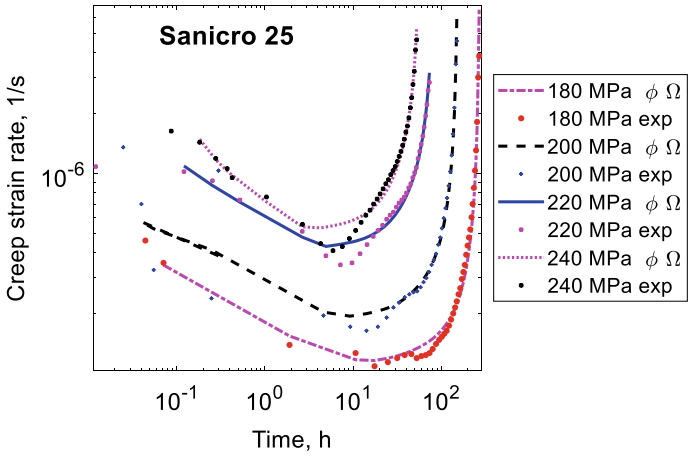


**Fig. 4.7** Creep rate versus time curves for the 22Cr25Ni4W1.5Co3CuNbN austenitic stainless steel Sanicro 25 at 750 °C for the same tests as in Fig. 4.5. Double logarithmic scale. Reprinted from [13] with permission of MDPI

The creep rates in Figs. 4.6, 4.7 and 4.8 show deviations to phi ($\phi$) and Omega ($\Omega$) model around the minimum creep rate. This is a common effect for many creep curves. The experimental values in the range are lower than the model values. These deviations are not large enough to show up in the creep strain curves in Fig. 4.5.

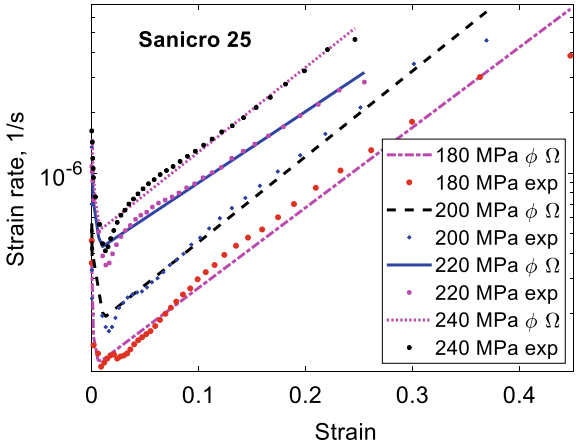


**Fig. 4.8** Creep rate versus strain curves for the 22Cr25Ni4W1.5Co3CuNbN austenitic stainless steel Sanicro 25 at 750 °C for the same tests as in Fig. 4.5. Semi logarithmic scale. Redrawn from [14] with permission of Taylor & Francis

The reason of modeling creep strain is in general to try to extrapolate the results to other conditions. This is typically very difficult with empirical methods. The background is that the fitting parameters practically always vary in a complex way that is challenging to analyze. Instead, the basic models that are described in the next three sections are readily useful to generalize the results to new conditions.

## 4.3 Dislocation Controlled Primary Creep

In Chap. 2, an expression for the creep rate in the secondary stage was derived, Eqs. (2.30) and (2.29)

$$\dot{\varepsilon} = h(\sigma - \sigma_i) \quad \text{with} \quad h(\sigma) = \frac{2\tau_L b c_L}{m_T} M(T,\sigma) \frac{\sigma^3}{(\alpha m_T G b)^3} \tag{4.3}$$

$$\sigma_{disl} = \alpha m_T G b \rho^{1/2} = \sigma - \sigma_i \tag{4.4}$$

where $\dot{\varepsilon}$ is the strain rate, $\sigma$ the applied stress, $m_T$ the Taylor factor, $b$ burgers vector, $G$ the shear modulus, $c_L$ and $\alpha$ dimensionless factors, $\omega$ the dynamic recovery constant, $\tau_L$ the dislocation line tension and $M$ the dislocation mobility. $\sigma_{disl}$ is the dislocation stress, $\rho$ the dislocation density, $\sigma_i$ is an internal stress that will be discussed below. Contributions from solid solution hardening and particle hardening can be included in $\sigma_i$. The validity of these equations was demonstrated in Chap. 2.

To derive the time dependence of the creep strain, the corresponding time dependence of the dislocation density must be known. Eq. (2.17) describes this variation

$$\frac{d\rho}{d\varepsilon} = \frac{m_T}{bc_L}\rho^{1/2} - \omega\rho - 2\tau_L M\rho^2/\dot{\varepsilon} \tag{4.5}$$

where ε is the strain. The other quantities were explained above.

The common behavior in the primary creep stage is that there is a continuously decreasing creep rate with increasing time until the secondary stage is reached. At the same time it is assumed that there is a gradually increasing density of dislocations. This is a natural assumption since the dislocation density is low at the start of the creep test for soft hot worked materials. The density reaches a stationary value in the secondary stage. There are many possible alternative scenarios for example with a hard cold worked material or continuous precipitation in the primary stage. However, we will only consider the main one.

To describe primary creep several assumptions are made [20]:

- The stress dependence of the creep rate is the same in the primary and in the secondary stage. This means that the function $h(\sigma)$ in Eq. (4.3) should be applicable.
- The development of the dislocation density can be described with the same equation, Eq. (4.5) that was used to derive the equation for the secondary creep rate.
- When starting from a low dislocation density at the start of the creep, Eq. (4.5) gives an increasing dislocation density. This density is assumed to generate a dislocation back stress according to Eq. (4.4).
- The creep rate in the primary stage is given by

$$\dot{\varepsilon} = h(\sigma + \sigma_{\text{disl sec}} - \sigma_{\text{disl}} - \sigma_i) \tag{4.6}$$

  where $\sigma_{\text{disl sec}}$ is the stress due to the dislocations (dislocation stress) in the secondary stage. In comparison to Eq. (4.3), the effective stress in Eq. (4.6) is raised by what we can call the primary stress $\sigma_{\text{prim}}$

$$\sigma_{\text{prim}} = \sigma_{\text{disl sec}} - \sigma_{\text{disl}} \tag{4.7}$$

The presence of $\sigma_{\text{prim}}$ in Eq. (4.6) raises the creep rate in comparison to the secondary stage, which is a characteristic feature of primary creep. When the secondary stage is reached, the dislocation stress $\sigma_{\text{disl}}$ is equal to $\sigma_{\text{disl sec}}$ and $\sigma_{\text{prim}}$ vanishes as it should. $\sigma_{\text{prim}}$ is a help quantity which makes it possible to model the creep rate in the primary stage. The applied stress σ is still constant.

- In the secondary stage there is a balance between the applied stress σ and the back stress from the dislocations $\sigma_{\text{dislsec}}$ plus the internal stress $\sigma_i$

$$\sigma = \sigma_{\text{disl sec}} + \sigma_i \tag{4.8}$$

  If Eq. (4.8) is applied, Eq. (4.6) can be rewritten as

$$\dot{\varepsilon} = h(2(\sigma - \sigma_i) - \sigma_{disl}) \tag{4.9}$$

The internal stress $\sigma_i$ has several contributions

$$\sigma_i = \sigma_y(T, \dot{\varepsilon}) + \sigma_{SSH} + \sigma_{PH} \tag{4.10}$$

where $\sigma_y$ is the temperature and strain rate dependent yield strength, $\sigma_{SSH}$ and $\sigma_{PH}$ the contributions from solid solution hardening and precipitation hardening that will be discussed in Chaps. 6 And 7.

It is important to recognize that the five assumptions do not involve any new functions or new parameters. It is simply assumed that the same basic dislocation mechanisms control both the primary and the secondary stage. A number of quantities such as the dislocation stresses $\sigma_{disl}$ and $\sigma_{dislsec}$ and contributions to the internal stress $\sigma_{SSH}$ and $\sigma_{PH}$ are mathematical quantities that are useful in the modeling. These quantities can be defined in different ways. It is important to recognize that these quantities cannot be measured and they are not meaningful unless they are precisely defined. For example, there are many ways of defining a back or internal stress. A general discussion about a back stress without a proper definition does not make sense.

In the contribution to the internal stress in Eq. (4.10), the yield strength has been included. It is possible to make exactly the same analysis about primary creep without taking the yield strength into account. It is material dependent if the yield strength should be taken into account.

The use of the model will now be illustrated for two creep tests of Cu-OFP. In Fig. 4.9 the development of the dislocation density, Eq. (4.5) and the dislocation stress, Eq. (4.4) are shown.

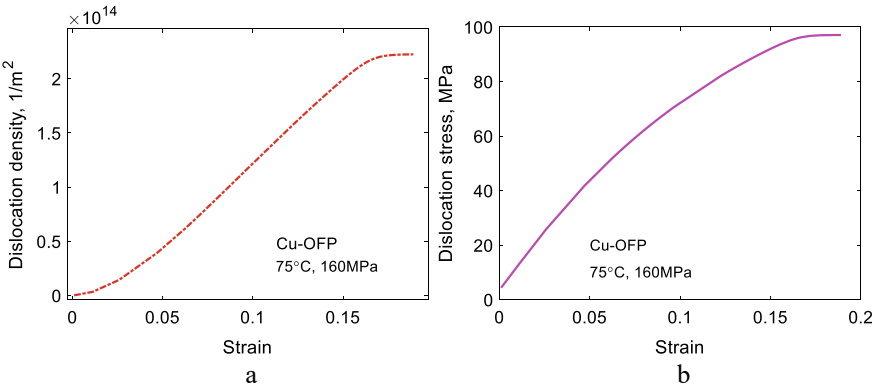


**Fig. 4.9** Creep test of Cu-OFP at 75 °C and 160 MPa. The creep test was interrupted after 12000 h; **a** dislocation density versus strain according to Eq. (4.5); **b** dislocation stress versus strain for the dislocation density in **a** according to Eq. (4.4)

The dislocation density increases approximately linearly with increasing strain over most of the strain range considered. When the dislocation density has reached a sufficiently high level, the third (static recovery) term gives a contribution. Eventually there is a balance between the two contributions. The secondary stage has been reached. At this stage the dislocation density becomes independent of strain. The dislocation stress, Eq. (4.4) is also continuously raised until a plateau in the secondary stage is reached. In the secondary stage the dislocation stress is the difference between the applied stress, 160 MPa, and the internal stress, Eq. (4.8). The internal stress consists of the yield strength and the solid solution hardening due to phosphorus and these quantities take the values 57 and 6 MPa, respectively at the temperature and strain rate of the test. The used model for solid solution hardening is presented in Chap. 6. In Fig. 4.9 the maximum dislocation stress is 97 MPa. These three values add up to the applied stress as they should according to Eq. (4.8).

In Fig. 4.10a the creep strain versus time curve for the same test is shown. It can be seen that the model can reproduce the observations even for the fast initial stage of the test.

The creep rate versus time is given in Fig. 4.10b. Also in this Figure it is evident that the model can describe the measurements. When the strain had reached a sufficiently high value in the test, the test had to be reloaded several times to avoid that the dead weights hit the floor. This is the reason for the spikes in the experimental curves.

In Fig. 4.10b with a double logarithmic scale, the data lie along a straight line in the primary stage. This indicates that copper in addition to P91 and Sanicro 25 follows the $\phi$ model, Eq. (4.1). It is evident that also the model, Eq. (4.9), shows this behavior.

The results for another creep test that has run until rupture are given Fig. 4.11. The general appearance of creep strain and creep rate curves is not very different from that in Fig. 4.10. Both the primary and secondary stages are reproduced by the model. The modeling of the tertiary stage which is not taken into account here will

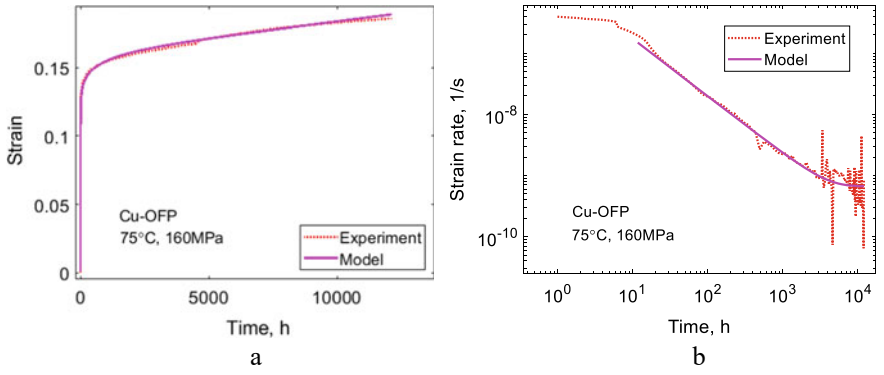


**Fig. 4.10** Creep test of Cu-OFP at 75 °C and 160 MPa. The creep test was interrupted after 12000 h; **a** creep strain versus time; **b** creep rate versus time; Eq. (4.9). Redrawn from [20] with permission of Elsevier

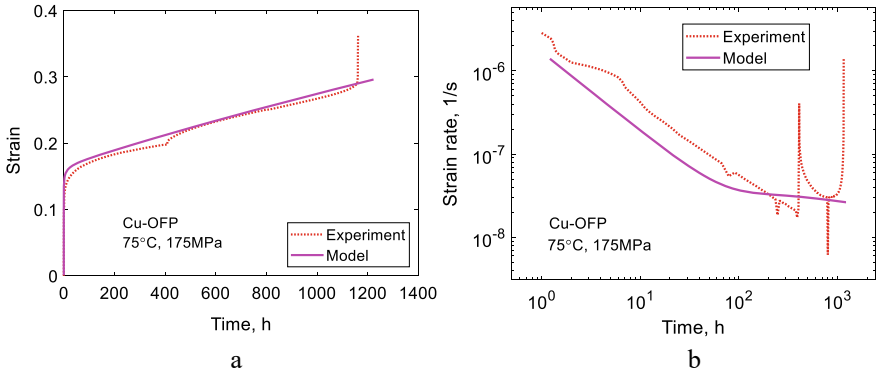


**Fig. 4.11** Creep test of Cu-OFP at 75 °C and 175 MPa. The creep test was run until rupture; **a** creep strain versus time; **b** creep rate versus time; Eq. (4.9)

be discussed in Chap. 12. Again the data and the model follow closely the phi ($\phi$) model in the primary stage.

## 4.4 Stress Adaptation

### *4.4.1 Model*

In Sect. 3.3 it was demonstrated that a stress strain curve which had the form of a Voce equation could be derived from Eq. (4.5)

$$\sigma = \sigma_y + (\sigma_{sat} - \sigma_y)(1 - \exp(-\omega\varepsilon/2)) \tag{4.11}$$

This relation can be rewritten as

$$\sigma_{sat} = \sigma_y + \frac{\sigma - \sigma_y}{1 - e^{-\omega\varepsilon/2}} \tag{4.12}$$

The saturation stress $\sigma_{sat}$ is closely related to the stationary creep stress. With this background, Eq. (4.12) is now generalized and transformed and considered as the driving stress for primary creep [4]

$$\sigma_{primSA} = \sigma_y(T, \dot{\varepsilon}) + \frac{\sigma - \sigma_y(T, \dot{\varepsilon})}{1 - e^{-\Omega\varepsilon/2}} \tag{4.13}$$

This expression is then inserted in Eq. (4.3) for the secondary creep rate

$$\frac{d\varepsilon}{dt} = h(\sigma_y(T, \dot{\varepsilon}) + \frac{\sigma - \sigma_y(T, \dot{\varepsilon})}{1 - e^{-\Omega\varepsilon/2}}, T) \tag{4.14}$$

The Ω value was originally identical to the dynamic recovery constant ω. However, it has been found that at situation far from stationary conditions, Ω might have to be chosen in a different way and that is discussed below. For this reason ω is replace by Ω in Eqs. (4.13) and (4.14). In Eq. (4.14) the yield strength depends on the temperature and the strain rate. The following dependence is assumed, Eq. (3.15).

$$\sigma_y(T, \dot{\varepsilon}) = \sigma_y(T_0, \dot{\varepsilon}_0)\frac{G(T)}{G(T_0)}\left(\frac{\dot{\varepsilon}}{\dot{\varepsilon}_0}\right)^{(1/n_N)} \tag{4.15}$$

$T_0$ is a reference temperature and $\dot{\varepsilon}_0$ a reference strain rate that are usually taken as 20 °C and $1 \times 10^{-4}$ 1/s, respectively. The temperature dependence of the yield strength follows that of the shear modulus *G*. The strain rate dependence is described with a Norton equation. $n_N$ is the stress exponent determined at the temperature and strain rate in question from the equation for the secondary creep rate, Eq. (2.30).

The expression for $\sigma_{primSA}$ is quite different from that of $\sigma_{prim}$ given in Sect. 4.3. Two features of Eq. (4.13) are important to recognize. When the strain increases $\sigma_{primSA}$ tends towards the applied stress and Eq. (4.14) is back to the expression for secondary creep. At small strains $\sigma_{primSA}$ can be expanded in the strain. If a Norton expression with a stress exponent is assumed, it can be shown that Eq. (4.14) takes the same form as Eq. (4.1) for the ϕ model. This means that if the ϕ model is valid for very small strains, Eq. (4.14) may be applicable. Equation (4.14) cannot be expected to be as general as the model in Sect. 4.3. Special assumptions are made and eq. (4.14) is based on the Voce equation that is not valid for all alloys. The strain rate and temperature dependence of the yield strength must be taken into account and they are not always known.

### *4.4.2 Numerical Integration*

Equation (4.14) is numerically complicated to integrate. The reason is that the yield strength depends on the strain rate. Thus in each integration step an iteration has to be performed. This way of direct integration is quite feasible. It is referred to as *stress adaptation* since to determine the stress $\sigma_{primSA}$ iteration is required in each step.

There are alternative ways to perform the integration. A brief summary is given here. For further details, see [21]. One way is to represent the function $h(\sigma, T)$ by a Norton equation

$$\frac{d\varepsilon}{dt} = h(\sigma, T) = A_N(T)\sigma^{n_N} \tag{4.16}$$

Using Eqs. (4.15) and (4.16), Eq. (4.14) can be rewritten as

$$\left(\frac{\dot{\varepsilon}}{A_{\mathrm{N}}}\right)^{1/n_{\mathrm{N}}} = \sigma_{\mathrm{y}}(T,\dot{\varepsilon}_0)\frac{G(T)}{G(T_0)}(\frac{\dot{\varepsilon}}{\dot{\varepsilon}_0})^{(1/n_{\mathrm{N}})} + \frac{\sigma - \sigma_{\mathrm{y}}(T,\dot{\varepsilon}_0)\frac{G(T)}{G(T_0)}(\frac{\dot{\varepsilon}}{\dot{\varepsilon}_0})^{(1/n_{\mathrm{N}})}}{1-e^{-\Omega\varepsilon/2}} \tag{4.17}$$

The following abbreviations are introduced

$$a_{\mathrm{N}} = A_{\mathrm{N}}^{1/n_{\mathrm{N}}} \qquad b_{\mathrm{N}} = \sigma_{\mathrm{y}}(T,\dot{\varepsilon}_0)\frac{G(T)}{G(T_0)}/\dot{\varepsilon}_0^{1/n_{\mathrm{N}}} \tag{4.18}$$

Using these abbreviations and solving for $\dot{\varepsilon}$ gives

$$\dot{\varepsilon}^{1/n_{\mathrm{N}}} = \frac{1}{1/a_{\mathrm{N}} - b_{\mathrm{N}} + \frac{b_{\mathrm{N}}}{1-e^{-\Omega\varepsilon/2}}}\ \frac{\sigma}{1-e^{-\Omega\varepsilon/2}} \tag{4.19}$$

From this expression, the formula for the yield strength can be obtained directly

$$\sigma_{\mathrm{y}}(T,\dot{\varepsilon}) = \sigma_{\mathrm{y}}(T,\dot{\varepsilon}_0)\frac{G(T)}{G(T_0)}\left(\frac{\dot{\varepsilon}}{\dot{\varepsilon}_0}\right)^{1/n_{\mathrm{N}}} = b_{\mathrm{N}}\dot{\varepsilon}^{1/n_{\mathrm{N}}} = \frac{\sigma}{(\frac{1}{a_{\mathrm{N}}b_{\mathrm{N}}}-1)(1-e^{-\Omega\varepsilon/2})+1} \tag{4.20}$$

The strain rate has now been eliminated so the integration of Eq. (4.14) can be performed directly. This procedure is referred to as *expansion integration.*

Another problem in the numerical integration is the singularity for small strains in Eqs. (4.14) and (4.20). This singularity can be eliminated by modifying the model in the following way [22]. In Eq. (4.13) the strain rate dependence is extracted

$$\sigma = \left[\sigma_{\mathrm{y}}(T) + K(T)(1-\mathrm{e}^{-\omega\varepsilon/2})\right](\frac{\dot{\varepsilon}}{\dot{\varepsilon}_{\mathrm{k}}})^{1/n_{\mathrm{N}}} \tag{4.21}$$

$\sigma_{\mathrm{y}}$ and $K$ are assumed to have the same strain rate dependence, which is approximately the case. The reference strain rate $\dot{\varepsilon}_{\mathrm{k}}$ is only known for the maximum stress, which also defines $K$

$$\dot{\varepsilon}_{\mathrm{k}} = A_{\mathrm{N}}(\sigma_{\mathrm{y}}(T) + K(T))^{n_{\mathrm{N}}} \tag{4.22}$$

$A_{\mathrm{N}}$ and $n_{\mathrm{N}}$ are determined from the total stress $\sigma_{\mathrm{primSA}}$ in Eq. (4.13) in the same way as in the previous integration alternative. From Eq. (4.21) an expression for the strain rate can be obtained

$$\frac{\dot{\varepsilon}}{\dot{\varepsilon}_{\mathrm{k}}} = \left\{\frac{\sigma}{\sigma_{\mathrm{y}}(T) + K(T)(1-\mathrm{e}^{-\Omega\varepsilon/2})}\right\}^{n_{\mathrm{N}}} \tag{4.23}$$

Equations (4.22) and (4.23) give

$$\dot{\varepsilon} = A_{\mathrm{N}}\left\{\frac{\sigma(\sigma_{\mathrm{y}}(T) + K(T))}{\sigma_{\mathrm{y}}(T) + K(T)(1-\mathrm{e}^{-\Omega\varepsilon/2})}\right\}^{n_{\mathrm{N}}} \tag{4.24}$$

The Norton Eq. (4.24) can be replaced by an equation of the original form, Eq. (4.14)

$$\dot{\varepsilon} = h\left( \frac{\sigma(\sigma_y(T) + K(T))}{\sigma_y(T) + K(T)(1 - e^{-\Omega\varepsilon/2})}, T \right) \tag{4.25}$$

In Eq. (4.25) the singularity at small strains has been removed. This procedure is referred to as *max stress integration.*

A simplistic variant of Eq. (4.25) will be given to illustrate how the model works [23]. The formula in Eq. (4.25) will be expressed as a Norton equation with the constants $A$ and $n$. Considering small strains ($\Omega\varepsilon/2 < 1$), the exponential can be expanded

$$\dot{\varepsilon}_{\text{prim}} = A\left\{ \frac{\sigma(1 + \sigma_y/K)}{\sigma_y/K + \Omega\varepsilon/2)} \right\}^n \tag{4.26}$$

Equation (4.26) is integrated with respect to time $t$. Assuming the initial strain to be zero, one finds that

$$\varepsilon = \{(1+n)A\}^{1/(n+1)} \left\{ \frac{2\sigma(1 + \sigma_y/K)}{\Omega} \right\}^{\frac{n}{n+1}} t^{\frac{1}{n+1}} - \frac{2\sigma_y}{K\Omega} \tag{4.27}$$

The time derivative of Eq. (4.27) is

$$\frac{d\varepsilon}{dt} = \frac{\{(1+n)A\}^{1/(n+1)}}{n+1} \left\{ \frac{2\sigma(1 + \sigma_y/K)}{\Omega} \right\}^{\frac{n}{n+1}} t^{-\frac{n}{n+1}} \tag{4.28}$$

Although Eqs. (4.26) and (4.28) are both derivatives of Eq. (4.27), they are not identical because Eq. (4.26) is a function of strain and Eq. (4.28) a function of time.

According to the simplistic model, the stress exponent is $n/(n+1)$, i.e. close to 1 provided $n$ is not small. The time dependence is also of importance. The $\phi$ model is valid for many materials in the primary stage

$$\dot{\varepsilon}_{\text{prim}\phi} = A_\phi t^{-\phi} \tag{4.29}$$

where $t$ is the time and $A_\phi$ and $\phi$ are parameters. Further details about the $\phi$ model can be found in Sect. 4.2 and in [22]. From (4.28) it can be seen that the simplistic model agrees with the $\phi$ model where $\phi = n/(n+1)$. This requires that the last term in (4.27) is small is relation to the value of the strain. This can be expressed in terms of the following criterion

$$\frac{\sigma_y}{K} < \frac{\Omega\varepsilon}{2} \tag{4.30}$$

It can be shown that this criterion must also be fulfilled for the full model in Eq. (4.25).

If the primary creep is near its end and approaching stationary conditions, Ω can be replaced with the dynamic recovery constant ω. The temperature correction for ω introduced in Sect. 3.4, $(G(\mathrm{RT})/G(T))^2$, where $G(T)$ and $G(\mathrm{RT})$ are the shear modulus at temperature and room temperature respectively, should be considered. However, if the primary creep is far from stationary conditions, Ω has to be determined in an other way [22]. At low strains the work hardening can be found from Eq. (3.12)

$$\frac{d\sigma_{\mathrm{disl}}}{d\varepsilon} = \frac{\alpha G m_{\mathrm{T}}^2}{2c_{\mathrm{L}}} \tag{4.31}$$

The dislocation stress can never be larger than the applied stress. When the dislocation stress is approaching the applied stress, a semi-stationary condition may be said to be reached. The strain has then the value

$$\varepsilon_{\mathrm{semi\ stat}} = (\sigma - \sigma_{\mathrm{i}})\frac{2c_{\mathrm{L}}}{\alpha G m_{\mathrm{T}}^2} \tag{4.32}$$

At this stage the exponential in Eq. (4.25) must be small, say 0.05, which gives

$$\Omega \approx \frac{3}{\varepsilon_{\mathrm{semi\ stat}}} = \frac{3\alpha G m_{\mathrm{T}}^2}{2c_{\mathrm{L}}(\sigma - \sigma_{\mathrm{i}})} \tag{4.33}$$

where $\sigma_{\mathrm{i}}$ includes strength contributions, for example, from solid solution and precipitation hardening. The applicability of Eq. (4.33) is shown for example in Sect. 5.8 and [22] for applications at a wide range of temperatures for copper.

### *4.4.3 Applications*

The use of Eq. (4.14) will now be illustrated. Two examples for creep tests of Cu-OFP at 75 °C are shown. The results for a test at a stress of 180 MPa are shown in Fig. 4.12.

It can be seen that the creep strain and creep strain rate versus time are approximately reproduced. The three integration methods stress adaptation, expansion integration and max stress integration give closely the same result. The straight line in Fig. 4.12b indicates that the phi (ϕ) model is followed down to fairly short times.

Another example is presented in Fig. 4.13. Again the experimental results for the creep strain and the creep rate are modeled in a general way. It is clear that the model in the present section gives a less precise description of the data than the model in Sect. 4.3. However, the model is useful to describe results at very low stresses, Chap. 5.

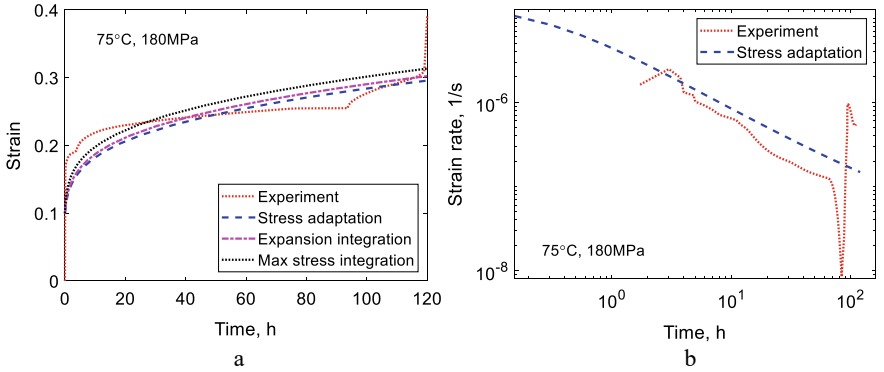


**Fig. 4.12** Creep test of Cu-OFP at 75 °C and 180 MPa. The creep test was run until rupture; **a** creep strain versus time; **b** creep rate versus time; Eq. (4.14)

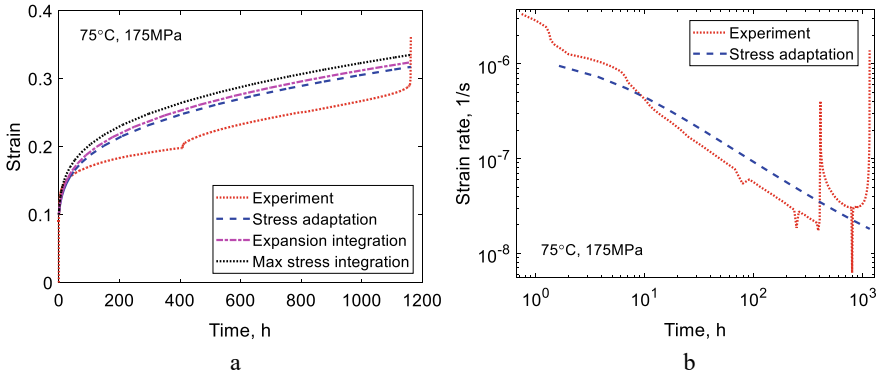


**Fig. 4.13** Creep test of Cu-OFP at 75 °C and 175 MPa. The creep test was run until rupture; **a** creep strain versus time; **b** creep rate versus time; Eq. (4.14)

## 4.5 12% Cr Steels

### *4.5.1 Dislocation Model*

The creep models presented in Sects. 4.3 and 4.4 as well as in Chap. 2 are based on a single dislocation density. However, there are materials for which more than one type of dislocation density must be introduced to fully take into account the role of the substructure. For the type of material, 9–12% Cr steels, that will be analyzed in this section, this is essential. In models with a single dislocation density, it is increased gradually from low values in the primary stage until it reaches the stationary value in the secondary stage. For 9–12% Cr steels, the initial microstructure is an annealed martensitic structure. It is characterized by well-developed subgrains with

subboundaries full of dislocations. This implies that the initial dislocation density is high. But the creep behavior of the 9–12% Cr steels in the primary stage is not very different from that in the fcc-alloys.

To handle this situation, a distinction is made between free and immobile dislocations. The free dislocations are located in the subgrain interiors and the immobile ones primarily in the subboundaries. The following equations are formulated for the densities of the free dislocations $\rho_f$ and the immobile dislocations $\rho_{im}$ [24, 25]

$$\frac{d\rho_f}{d\varepsilon} = \frac{1}{L_s}\frac{m_T}{b} - (\omega_1 + \omega_2)\rho_f \tag{4.34}$$

$$\frac{d\rho_{im}}{d\varepsilon} = \omega_2\rho_f - 2M\tau_L\rho_{im}^2/\dot{\varepsilon} \tag{4.35}$$

ε is the strain, $\dot{\varepsilon}$ the creep rate, $L_s$ the mean spurt distance of dislocations, $m_T$ the Taylor factor, $b$ Burgers vector, $M$ the climb mobility, and $\tau_L$ the dislocation line tension. The first term on the right hand side of Eq. (4.34) gives the work hardening. Only the free dislocations contribute to the work hardening. There are two types of dynamic recovery. A free dislocation will interact with a dislocation of opposite Burgers creating a dipole with a spacing $d_{dip}$ that can annihilate each other

$$d_{dip} = \frac{m_T}{8\pi(1-\nu_P)}\frac{Gb}{\sigma} \tag{4.36}$$

This gives a recovery constant $\omega_1$

$$\omega_1 = \frac{2m_T}{b}\frac{d_{dip}}{n_{slip}} \tag{4.37}$$

$n_{slip}$ is the number of active slip systems. Dislocations can also form locks, when dislocations with different Burgers vector at a distance of $d_{lock}$ interact. $d_{lock}$ has about the same size as $d_{dip}$. This is another recovery effect that transfers the free dislocations to immobile ones.

$$\omega_2 = \frac{4m_T}{b}\frac{d_{lock}\left(n_{slip}-1\right)}{n_{slip}} \tag{4.38}$$

Thus this type of recovery reduces the free dislocation density and increases the immobile dislocation density. It gives no net change in the total dislocation density. The immobile dislocations can only be removed by static recovery. The static recovery term is the last term in Eq. (4.35) and it has the same form as in Eq. (4.5).

Only the immobile dislocations are included in Eq. (4.39) for the dislocation stress

$$\sigma_{disl} = \alpha m_T G b \rho_{im}^{1/2} \tag{4.39}$$

It is now possible to describe what happens during primary creep. Initially, $\rho_f$ has a high value and $\rho_{im}$ a low value. This gives a high total dislocation density, but the dislocation stress is low. To compute the strain rate, $\sigma_{disl}$ should be inserted in Eq. (4.9). With a low value of $\sigma_{disl}$, the creep rate will be high. With increasing strain, the free dislocations are transferred to immobile ones, $\sigma_{disl}$ is increased and the creep rate reduced. With Eqs. (4.34) and (4.35) the established features of primary creep are reproduced.

The internal stress is an important quantity for 9–12% Cr-steels. Particles increase the creep strength in two ways. Fine carbo-nitrides give a direct increase in the creep strength. Coarse $M_{23}C_6$ carbides stabilize the subboundaries and thereby reduce the recovery rate of the immobile dislocations. This implies a high value of the dislocation strength can be kept that decreases the creep rate. Only the role of the fine carbo-nitrides will be discussed briefly here. Further details are given in Chap. 7 on precipitation hardening. Only particles with a radius larger than a critical size contribute to the creep strength, Eq. (7.12)

$$r_{crit} = M_{climb}(T, \sigma) b^2 \sigma \lambda_s \frac{\rho_f}{\dot{\varepsilon}_{sec} m_T} \tag{4.40}$$

where $\lambda_s$ is the interparticle spacing for all the carbo-nitrides. The particles give the following contribution to the internal stress

$$\sigma_i = \sigma_{part} = \frac{C_O G b m_T}{\lambda_{crit}} \tag{4.41}$$

where $C_O = 0.8$ and $\lambda_{crit}$ is the interparticle spacing for particles larger than $r_{crit}$. Equation (4.41) is the expression for the Orowan strength except that $\lambda_s$ is replaced by $\lambda_{crit}$. Together with $\sigma_{disl}$, $\sigma_i$ should be inserted in Eq. (4.9) to find the creep rate.

### 4.5.2 Simulated Creep Curves

Results for creep strain curves of 12Cr1MoV steels (X20) will be presented. The creep curves have been published in [9]. Two heats CL and CT are considered. The particles in this steel are primarily $M_{23}C_6$ carbides. M stands mainly for Cr and Fe. The size distribution of the carbides has been measured [26]. The result is presented in Fig. 4.14.

In the semi logarithmic scale in Fig. 4.14, the size distributions are approximately linear except for small particle sizes. The deviation for small particles is often due to the difficulty to make accurate measurements for such particles. Otherwise the Figure shows that the number of particles per unit area $n_{part}$ decreases exponentially with increasing carbide radius $r_{part}$

$$n_{part} = n_0 e^{-\beta r_{part}} \tag{4.42}$$

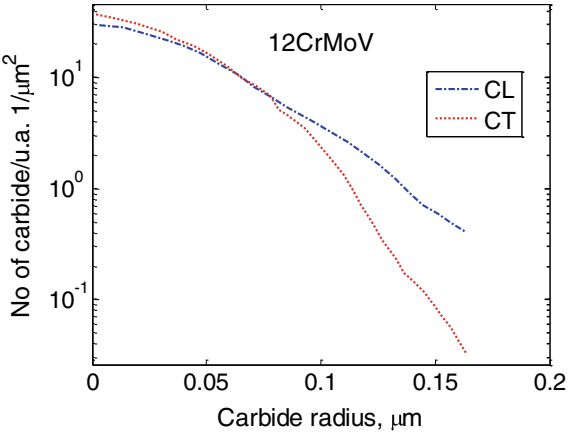


**Fig. 4.14** Number of $M_{23}C_6$ carbides per unit area versus carbide radius for two heats CL and CT for a 12Cr1MoV steels. From [27]

where $n_0$ and β are constants. The values of β for the heats CL and CT in Fig. 4.14 are $3.2 \times 10^7$ and $6.0 \times 10^7$ 1/m, respectively.

The initial values of the dislocation densities $\rho_f$ and $\rho_{im}$ have been taken as $8 \times 10^{13}$ and $1 \times 10^{11}$ 1/m$^2$ from two doctorial theses from Erlangen on 9 to 12% Cr-steels (Polcik 1998; Sailer 1998).

Experimental creep strain versus time curves are compared to the model in Figs. 4.15 and 4.16. The model curves only include primary and secondary creep since tertiary creep is not considered. In the primary and the secondary stages the experimental data is reasonably well reproduced.

This is further illustrated in Fig. 4.17 where the experimental and modeled minimum creep rates are compared. The Figure shows that the deviation is about a factor of two, which can be considered as acceptable. Again it is shown that primary creep can be accurately modeled without the use of adjustable parameters

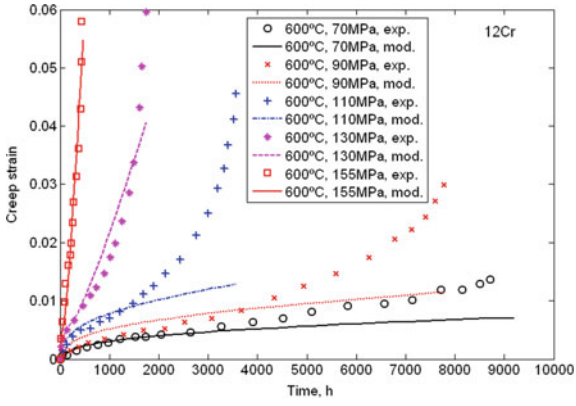


**Fig. 4.15** Creep strain versus time curves for 12CrMoV steel at 600 °C for stresses between 70 and 155 MPa. Experimental data from [9]. Heat CT. From [27]

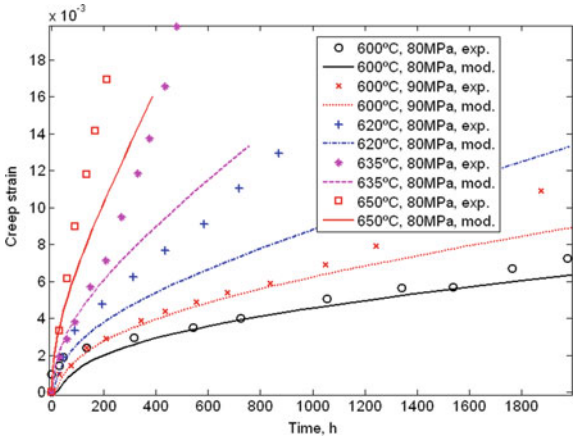


**Fig. 4.16** Creep strain versus time curves for 12CrMoV steel at 600–650 °C for a stress of 80 or 90 MPa. Experimental data from [9]. Heat CL. From [27]

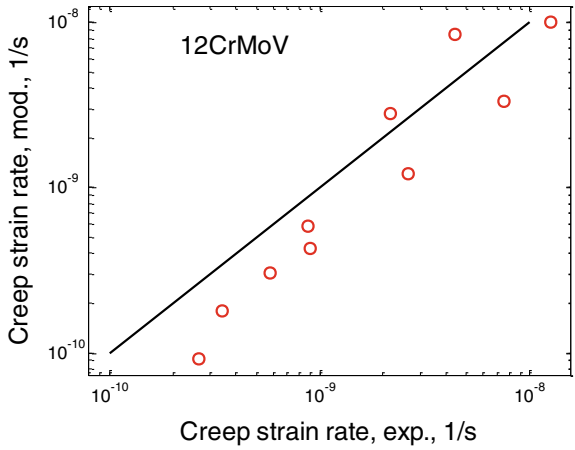


**Fig. 4.17** Comparison of minimum creep strain rates between the experimental and model curves in Figs. 4.15 and 4.16. From [27]

## 4.6 Summary

- Many empirical models exist for representing creep curves, i.e. creep strain versus time curves. With four or more parameters almost any of these models can give a good fit to the curves. To get a better basis for selection of models, primary and tertiary creep should be handled separately. Then it is enough to involve just two parameters for primary creep and two for tertiary. For many types of steels primary creep can be represented with the phi model and tertiary creep with the Omega model. The phi model gives a linear curve in a double logarithmic strain rate versus time diagram. The Omega-model provides a linear curve when the logarithmic of the strain rate is shown as a function of the strain. The two models can be added to describe the whole creep curve. It is usually not necessary to have a separate term for secondary creep.

- Several basic models for primary creep are derived in the chapter. The modeling is based on the assumption that the dislocation density has initially a low value that increases during the primary stage until a stationary value is reached in the secondary stage that can be described with the basic dislocation models. The dislocation density is associated with a dislocation stress according to Taylor's equation. In one of the models an effective creep stress is introduced which is twice the applied stress minus the dislocation stress. This effective stress can be introduced in the expression for the secondary creep rate to find the creep rate in the primary stage. The expression can be generalized to include also tertiary creep, see Sect. 12.4.
- The use of the basic models for primary creep demonstrates that they can describe experimental creep curves. These modelled creep curves follow the phi model.
- For martensitic 9–12% Cr steels the situation is somewhat more complicated. Due to the martensitic microstructure the initial dislocation density is high. To handle this case at least two types of dislocation densities must be introduced; free and immobile. As a consequence, the development of both types of dislocations must be taken into account but the principles are the same.

## References

1. R. Wu, R. Sandstrom, F. Seitisleam, Influence of extra coarse grains on the creep properties of 9% CrMoV (P91) steel weldment. J. Eng. Mater.-T ASME **126**, 87–94 (2004)
2. S.R. Holdsworth, F. Abe, T.-U. Kern, R. Viswanathan, 14-Constitutive equations for creep curves and predicting service life, in *Creep-Resistant Steels* (Woodhead Publishing, 2008), pp. 403–420
3. S.R. Holdsworth, M. Askins, A. Baker, E. Gariboldi, S. Holmstrom, A. Klenk, M. Ringel, G. Merckling, R. Sandstrom, M. Schwienheer, S. Spigarelli, Factors influencing creep model equation selection. Int J Pres Ves Pip **85**, 80–88 (2008)
4. R. Sandstrom, Basic model for primary and secondary creep in copper. Acta Mater. **60**, 314–322 (2012)
5. R.W. Evans, B. Wilshire, in *Creep of Metals and Alloys* (Institute of Metals, Swansea, 1985)
6. P.G. McVetty, Factors affecting the choice of working stresses for high temperature service. Trans ASME **55**, 99 (1933)
7. D. McHenry, A new aspect of creep in concrete and its application to design. Proc. ASTM **43**, 1069 (1943)
8. A. Graham, K.F.A. Walles, Relations between long and short time properties of commercial alloys. J. Iron Steel Inst. **179**, 105–120 (1955)
9. R. Wu, R. Sandstrom, J. Storesund, Creep strain behavior in a 12%-Crmov steel. Mater. High Temp. **12**, 277–283 (1994)
10. R. Sandstrom, A. Kondyr, Creep deformation, accumulation of creep rupture damage and forecasting of residual life for three Mo- and CrMo-steels. VGB Kraftwerkstechnik **62**, 802–813 (1982)
11. R. Sandstrom, A. Kondyr, Model for tertiary Creep in Mo and CrMo steels, in *ICM 3* (Pergamon Press, 1979), pp. 275–228
12. M. Prager, Development of the MPC omega method for life assessment in the creep range. J. Pressure Vessel Technol. Trans. ASME **117**, 95–103 (1995)
13. R. Sandström, Basic analytical modeling of creep strain curves. Materials **16** (2023)

14. R. Sandström, J.-J. He, Prediction of creep ductility for austenitic stainless steels and copper. Mater. High Temp. *39*(6), 427–435 (2022)
15. F. Abe, Analysis of creep rates of tempered martensitic 9%Cr steel based on microstructure evolution. Mater. Sci. Eng. A **510–511**, 64–69 (2009)
16. F. Abe, Bainitic and martensitic creep-resistant steels. Curr. Opin. Solid State Mater. Sci. **8**, 305–311 (2004)
17. F. Abe, T. Horiuchi, M. Taneike, K. Sawada, Stabilization of martensitic microstructure in advanced 9Cr steel during creep at high temperature. Mater. Sci. Eng. A **378**, 299–303 (2004)
18. F. Abe, Coarsening behavior of lath and its effect on creep rates in tempered martensitic 9Cr–W steels. Mater. Sci. Eng. A **387–389**, 565–569 (2004)
19. Y. Zhang, H. Jing, L. Xu, L. Zhao, Y. Han, J. Liang, Microstructure and texture study on an advanced heat-resistant alloy during creep. Mater. Charact. **130**, 156–172 (2017)
20. R. Sandström, The role of cell structure during creep of cold worked copper. Mater. Sci. Eng. A **674**, 318–327 (2016)
21. R. Sandstrom, S. Waqas Ahmad, K.T. Pasupuleti, M. Mahdavi Shahri, Slow strain rate tensile testing of friction stir welded Cu-OFP. Constitutive equations for creep. Swedish Nuclear Waste Management Company Report R-13-33 (2017)
22. R. Sandström, Primary creep at low stresses in copper. Mater. Sci. Eng.: A (2023)
23. R. Sandström, Creep at low stresses in aluminium (Harper-Dorn) and in an austenitic stainless steel with a stress exponent of 1. Mater. Today Commun. **36** (2023)
24. F. Roters, D. Raabe, G. Gottstein, Work hardening in heterogeneous alloys—A microstructural approach based on three internal state variables. Acta Mater. **48**, 4181–4189 (2000)
25. H. Magnusson, R. Sandstrom, Creep strain modeling of 9–12 pct Cr steels based on microstructure evolution. Metall. Mater. Trans. A **38A**, 2033–2039 (2007)
26. R. Wu, R. Sandstrom, Carbide coarsening during creep in 12% CrMoV steel. J. Eng. Mater.-T ASME **118**, 485–492 (1996)
27. R. Sandstrom, H. Magnusson, Basic model for creep deformation in 12Cr1MoV steels, in *12th International Conference on Creep and Fracture of Engineering Materials and Structures Japan Institute of Metals* (2012)